Pergamon

Int. J. Multiphase Flow Vol. 24, No. 4, pp. 563–585, 1998

Printed in Great Britain

PII: S0301-9322(97)00082-7

0301-9322/98 $19.00 + 0.00

A SHEAR FLOW AROUND A SPINNING SPHERE: NUMERICAL STUDY AT MODERATE REYNOLDS NUMBERS

M. BEN SALEM and B. OESTERLE†

LUMEN (Laboratoire Universitaire de Mécanique et d'Energétique de Nancy), ESSTIN, Université Henri Poincaré—Nancy 1, 54500 Vandoeuvre-les-Nancy, France

(Received 21 March 1997; in revised form 29 October 1997)

Abstract—In order to contribute to the existing knowledge of the hydrodynamic forces exerted on a spinning spherical particle, the influence of combined shear and rotation on the lift, drag and torque is numerically investigated. The Navier–Stokes equations are solved using a finite volume formulation based on a pressure correction procedure. The accuracy of the numerical code is tested through comparison with theoretical results at small Reynolds numbers and with accepted numerical and experimental results for a uniform flow at moderate Reynolds numbers. The study is resticted to Reynolds numbers Re_p (based on sphere radius) up to 20, dimensionless shear rates $-0.3 \leq \chi^+ \leq +0.3$ and dimensionless angular velocities $-2 \leq \omega^+ \leq +2$. At small Reynolds numbers, it is found that the lift force on a spinning sphere in a linear shear flow can be obtained by superposing Saffman's or McLaughlin's results and Rubinow and Keller's results. Compared with the case of uniform flow, the drag is slightly affected by the shear rate, but is not altered by the rotation of the sphere, provided that the characteristic Reynolds numbers be small enough. At higher Reynolds numbers, the numerically predicted drag and lift coefficients were found to be significantly affected by the grid parameters, so that reliable results are restricted to the torque, which has not been studied by any author yet at particle Reynolds numbers exceeding unity. A correlation for the torque coefficient versus the parameters Re_p, χ^+ and ω^+ is finally proposed.

Key Words: spinning sphere, shear flow, particles, drag force, lift force, hydrodynamic torque

1. INTRODUCTION

Studies concerning the numerical simulation of two-phase flows have become more and more important in recent years and significant progress has been made on the prediction of such flows. Among them, the fluid–solid suspension flows, which are important for many industrial application, are often predicted by means of so-called Lagrangian simulation techniques, which are based on the computation of a large number of particle trajectories. In some kinds of confined suspension flows, solid particles may undergo significant transverse forces, due to the collision induced spinning motion and to the large fluid velocity gradient in the near-wall region. In order to carry out trajectory computations in such flows, it is thus necessary to know the force and the torque undergone by the particles, which are of decisive importance. It was therefore decided to investigate the force and the torque acting on spherical particle under influence of both spin and shear. Generally, the particles are not spherical and their shape undoubtedly affects the forces which act on them. Nevertheless, the sphere is the only shape for which results can be generalized without regard to attitude and it is therefore the natural choice for investigation.

In reviewing the literature, it can be seen that only few works deal with the problem of a spinning sphere that translates in a shear flow. The first results concerning the forces exerted by the fluid on a spherical particle in a non-uniform steady flow were obtained by Faxen (see Feuillebois, 1980) by neglecting the inertia terms. Bretherton (1962) proved that if such inertia terms are neglected, no transverse force can exist for a body of revolution in a unidirectional flow. Rubinow and Keller (1961) and Saffman (1965, 1968) both used asymptotic expansions to

†To whom correspondence should be addressed.

obtain inertial corrections for small values of the Reynolds number in the case of a solid sphere in an unbounded flow domain. Saffman (1965, 1968) derived an expression for the lift force on a small sphere in a linear shear flow.This expression is valid when the three Reynolds numbers defined by $Re_p = aV/v$, $Re_\chi = a^2|\chi|/v$ and $Re_\omega = a^2|\omega|/v$ satisfy the conditions:

$$Re_p \ll Re_\chi^{1/2} \ll 1 \text{ and } O(Re_\omega) = O(Re_\chi), \quad [1]$$

where a denotes the particle radius, v is the fluid viscosity, χ is the velocity gradient, ω is the angular velocity and V denotes the magnitude of the particle slip velocity, which refers to the sphere centre velocity relative to the undisturbed fluid velocity at that point. Saffman's theory, which shows that the rotation induced lift force is an order of magnitude lower than the shear induced lift force if [1] is fullfilled, was recently extended by McLaughlin (1991). He investigated other cases in which the particle Reynolds number Re_p based on the slip velocity is comparable with or larger than the square root of the Reynolds number Re_χ based on the velocity gradient. Both of these Reynolds numbers are small in magnitude compared with unity. More recently, Cherukat *et al.* (1994) experimentally studied the shear-induced inertial migration of a rigid sphere using a homogeneous shear apparatus. Their experimental results, obtained for a range of slip Reynolds numbers $Re_p = 0.1$–2.5 indicate that McLaughlin's expression for the inertial lift, which reduces to Saffman's expression for large values of the parameter $\xi = Re_\chi^{1/2}/Re_p$, may be used to predict the lift force when $Re_p < 1$.

The above analyses are restricted to small particle Reynolds numbers. Auton (1987) has derived an expression of the lift force on a sphere in a weak shear flow of an inviscid fluid when the change in the incident velocity of the undisturbed flow field across the sphere is small compared with the relative velocity of the sphere. At moderate particle Reynolds numbers Re_p, ranging up to 50, Dandy and Dwyer (1990) performed a numerical calculation of the lift and drag forces on a fixed sphere in a shear flow. Their results concerning the lift have been correlated by Mei (1992) who proposed an approximate relationship for the shear lift force on a spherical particle by expressing the lift coefficient at finite Reynolds numbers in terms of the theoretical lift coefficient of Saffman. Nevertheless, the numerical calculations of Dandy and Dwyer (1990) must be interpreted with caution since the accuracy of their lift predictions was checked by comparing their results at small Reynolds numbers to the solution of Saffman, whithout meeting the conditions given above by [1]. For such a comparison, they considered the case $Re_p = 0.05$ and six values of the dimensionless shear rate $\chi^+ = a\chi/V$: 0.01, 0.025, 0.05, 0.1, 0.2 and 0.4. When we calculate, for instance, Re_χ for $\chi^+ = 0.025$, we find that $Re_p > Re_\chi^{1/2}$ (Re_χ is related to Re_p by $Re_\chi = \chi^+ Re_p$). It can be shown for this example that the error is 44% by comparison with the theoretical result of McLaughlin (1991) who made the only assumption that Re_p and Re_χ are small compared with unity. Morever, in the study by Dandy and Dwyer (1990), the outer boundary radius was only 25 radii of the sphere, a value which seems not to be large enough to achieve reliable predictions at low Reynolds numbers.

It must be emphasized that the sphere rotation was not taken into account in most of the above-mentioned works and that no information can be found concerning the torque undergone by a sphere in a shear flow at moderate Reynolds numbers. However, works dealing with the case of a spinning sphere placed in a uniform fluid flow can be found in the literature. Regarding this problem, the range of small Reynolds number was theoretically investigated by Rubinow and Keller (1961) who took into account the inertia terms in analysing the steady flow aroud a rotating sphere by the means of matched asymptotic expansions. Higher-order expansions were derived by Takagi (1974), but such expansions diverge quickly as soon as Re_p exceeds unity. At finite Reynolds numbers, this problem was numerically investigated by Chegroun (1992) who computed the drag, lift and torque coefficients of a translating and spinning sphere in the range of particle Reynolds numbers Re_p up to 20. Her numerical results have been compared with good agreement to the measurements of Oesterle and Bui Dinh (1998) who used a trajectography technique to investigate the problem in the range of particle Reynolds numbers $0 \leq Re_p \leq 65$.

To the best of the authors' knowledge, it can be concluded that there is no expression available as yet for the lift and drag forces and for the torque exerted on a spinning particle in a shear flow. In this paper, we propose a numerical study of such a problem in restricting ourselves to the case of a spinning spherical particle suspended in a uniform unbounded linear shear flow in the range $Re_p \leq 20$. The text will be divided into three parts. The formulation of the problem is presented in the first part. The second part is devoted to the description of the outlines of the numerical procedure. In the third part, the accuracy of the numerical technique is tested by comparing our results with accepted ones in the literature and original results, concerning mainly the dimensionless torque, which was not studied by any author yet, are presented and discussed.

2. PROBLEM FORMULATION

We consider the steady motion of a solid sphere in a linear shear flow. The spherical particle is assumed to be rigid so that it has a no-slip surface. It is convenient to state the problem in a frame of reference moving with the particle, so that the fluid velocity is time-independent. The undisturbed fluid velocity is described by:

$$\mathbf{V}_\infty(x) = (V + \chi x)\mathbf{k}, \tag{2}$$

where $\mathbf{k}$ is the unit vector of the z-direction, χ is a constant shear rate and V is the undisturbed constant fluid velocity at the sphere centre, which is located at $x = 0$. As shown by figure 1, which schematizes the problem, the angular velocity of the sphere, which is also constant, is assumed to be orthogonal to the directions of the flow and of the velocity gradient and can thus be written as:

$$\mathbf{\Omega} = \omega \mathbf{j}, \tag{3}$$

where $\mathbf{j}$ is the unit vector in the y-direction. The sphere Reynolds numbers considered in this work lie in the range $Re_p \leq 20$, so that the flow is described by the full Navier–Stokes equations, which are written, with the connected boundary conditions, in a spherical polar coordinate system. In steady-state conditions, these equations can be expressed under the following conservative form:

$$\frac{1}{r^2}\frac{\partial(r^2\mathbf{F})}{\partial r} + \frac{1}{r\sin\theta}\frac{\partial(\mathbf{G}\sin\theta)}{\partial\theta} + \frac{1}{r\sin\theta}\frac{\partial\mathbf{H}}{\partial\phi} = \mathbf{S}, \tag{4}$$

where $\mathbf{S}$ is the source vector and $\mathbf{F}$, $\mathbf{G}$ and $\mathbf{H}$ are the flux vectors. These vectors are expressed in terms of the unknowns of the problem, which are the velocity components (u, v, w) and the pressure p, by:

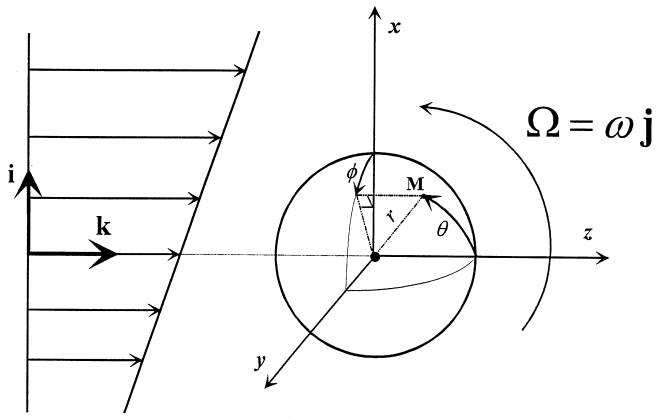

Figure 1. Problem geometry.

$$\mathbf{F} = \begin{bmatrix} u^2 - \dfrac{2}{Re_p}\dfrac{\partial u}{\partial r} + p \\ uv - \dfrac{2}{Re_p}\dfrac{\partial v}{\partial r} \\ uw - \dfrac{2}{Re_p}\dfrac{\partial w}{\partial r} \end{bmatrix}, \quad [5]$$

$$\mathbf{G} = \begin{bmatrix} uv - \dfrac{2}{rRe_p}\dfrac{\partial u}{\partial \theta} + \dfrac{4v}{rRe_p} \\ v^2 + p - \dfrac{2}{rRe_p}\dfrac{\partial v}{\partial \theta}\dfrac{4u}{rRe_p} \\ vw - \dfrac{2}{rRe_p}\dfrac{\partial w}{\partial \theta} \end{bmatrix}, \quad [6]$$

$$\mathbf{H} = \begin{bmatrix} uw - \dfrac{2}{rRe_p \sin\theta}\dfrac{\partial u}{\partial \phi} + \dfrac{4w}{rRe_p} \\ vw - \dfrac{2}{rRe_p \sin\theta}\dfrac{\partial v}{\partial \phi} + \dfrac{4w}{rRe_p \tan\theta} \\ w^2 + p - \dfrac{2}{rRe_p \sin\theta}\dfrac{\partial w}{\partial \phi} - \dfrac{4}{Re_p}\left(\dfrac{u}{r} + \dfrac{v}{r\tan\theta}\right) \end{bmatrix}, \quad [7]$$

$$\mathbf{S} = \begin{bmatrix} \dfrac{v^2 + w^2}{r} + \dfrac{2p}{r} - \dfrac{4u}{r^2 Re_p} \\ \dfrac{w^2}{r\tan\theta} - \dfrac{uv}{r} + \dfrac{p}{r\tan\theta} - \dfrac{2}{r^2 Re_p}\left(\dfrac{v}{\sin^2\theta} + \dfrac{2u}{\tan\theta}\right) \\ -\dfrac{vw}{r\tan\theta} - \dfrac{uw}{r} - \dfrac{2w}{r^2 Re_p \sin^2\theta} \end{bmatrix}. \quad [8]$$

In addition, the velocity components must satisfy the continuity equation:

$$\frac{1}{r^2}\frac{\partial}{\partial r}(r^2 u) + \frac{1}{r\sin\theta}\frac{\partial}{\partial \theta}(v\sin\theta) + \frac{1}{r\sin\theta}\frac{\partial w}{\partial \phi} = 0. \quad [9]$$

The above equations are written in a dimensionless form by using the radius a of the spherical particle as a characteristic length, the centreline velocity V as a characteristic velocity and ρV^2 as a pressure scale:

$$r = \frac{r'}{a},\ u = \frac{v_r}{V},\ v = \frac{v_\theta}{V},\ w = \frac{v_\phi}{V},\ p = \frac{p'}{\rho V^2}, \quad [10]$$

where v_r, v_θ and v_ϕ are the dimensional components of the velocity vector in the curvilinear coordinate system, r' is the actual polar radius of the particle, p' is the actual pressure and ρ is the fluid density.

The velocity boundary condition at infinity, i.e. at the outer boundary of the computational domain, is:

$$\mathbf{V} \longrightarrow \mathbf{V}_\infty \text{ as } r \longrightarrow \infty, \quad [11]$$

and the no-slip condition at the sphere surface is given by

$$\mathbf{V} = \boldsymbol{\Omega} \times \boldsymbol{r} \text{ at } r = 1. \quad [12]$$

Because of the symmetry against the xz-plane, we will consider only the half of the computational domain, i.e. $0 \le \theta \le \pi$ and $0 \le \phi \le \pi$. It is therefore necessary to write the boundary

conditions for $\theta = 0$, $\theta = \pi$, $\phi = 0$ and $\phi = \pi$. The symmetry implies that:

$$\frac{\partial u}{\partial \phi} = \frac{\partial v}{\partial \phi} = w = 0 \text{ for } \phi = 0 \text{ and } \phi = \pi, \quad [13]$$

and that the velocity component normal to the symmetry plane must vanish for all ϕ on the axis, leading to

$$v \sin \phi + w \cos \phi = 0 \text{ for } \theta = 0, \quad [14]$$

$$-v \sin \phi + w \cos \phi = 0 \text{ for } \theta = \pi. \quad [15]$$

Moreover, for $\theta = 0$ and $\theta = \pi$ (i.e. on the z-axis), the radial velocity component u is directed by the z-direction and is therefore independent of ϕ, so that we have:

$$\frac{\partial u}{\partial \phi} = 0 \text{ for } \theta = 0 \text{ and } \theta = \pi. \quad [16]$$

3. METHOD OF SOLUTION

3.1. *Grid*

In order to obtain solutions for $\mathbf{V}(r, \theta, \phi)$ and $p(r, \theta, \phi)$, the governing equations are discretized on a spherical staggered grid, which is uniform in the angular directions, but non-uniform in the radial direction. In order that the mesh width be fine enough near the sphere surface, where the velocity gradient is expected to be the steepest, the grid spacing in the radial direction is increasing towards the outer boundary of the flow, according to the following exponential law:

$$r_i = \exp[(i-1)h]; \; i = 1, n_i, \quad [17]$$

$$\Delta r_i = r_i - r_{i-1} = r_i(1 - \mathrm{e}^{-h}); \; i = 2, n_i, \quad [18]$$

where h denotes a dimensionless space step parameter. The internode spacing is constant in the θ and ϕ directions, the node coordinates being defined by:

$$\theta_j = \left(j - \frac{3}{2}\right)\Delta\theta; \; j = 2, n_j, \quad [19]$$

$$\phi_k = \left(k - \frac{3}{2}\right)\Delta\phi; \; k = 2, n_k \quad [20]$$

where $\Delta\theta$ and $\Delta\phi$ are the angular steps

$$\Delta\theta = \frac{\pi}{n_j - 1}, \; \Delta\phi = \frac{\pi}{n_k - 1} \quad [21]$$

The unknown pressures $p_{i,j,k}$ are located at the centre of the control volumes:

$$p_{i,j,k} = p\left(r_i - \frac{\Delta r_i}{2}, \theta_j, \phi_k\right), \quad [22]$$

whereas the components of the velocity vector are located at the centre of the control volume faces that are normal to them

$$u_{i,j,k} = u(r_i, \theta_j, \phi_k), \quad [23]$$

$$v_{i,j,k} = v\left(r_i - \frac{\Delta r_i}{2}, \theta_j + \frac{\Delta\theta}{2}, \phi_k\right), \quad [24]$$

$$w_{i,j,k} = w\left(r_i - \frac{\Delta r_i}{2}, \theta_j, \phi_k + \frac{\Delta\phi}{2}\right). \quad [25]$$

3.2. *Numerical procedure*

Computation is performed by means of a finite volume approach based on a pressure correction procedure. The momentum equations are discretized by integration of [4] on the appropriate staggered control volumes. The discretized equations are then solved through a line-by-line technique, after the convection terms have been linearized using the best available estimates of the velocity components, yielded by the previous iteration. These tentative values do not satisfy the mass conservation since computation is not started with the exact pressure field. Therefore, after each iteration, the velocity and pressure fields are approximately corrected by solving the pressure correction equation using the Simplex approach described by van Doormaal and Raithby (1985) in order that the resulting velocities and pressures ensure satisfaction for both momentum and continuity equations. This procedure is repeated until convergence is achieved. It is well known that the convection terms may be the source of numerical instabilities when the Peclet number becomes too large. In order to avoid such a problem, which may occur far from the sphere, where the internode spacing becomes more and more greater, a power-law scheme is used for the discretization of the convection terms (Patankar 1980). As is common when using a staggered grid, fictitious velocity components are calculated outside the computation domain in order to satisfy the boundary conditions.

Once converged velocity and pressure fields have been obtained for specified values of the flow parameters (which are the three Reynolds numbers Re_p, Re_χ and Re_ω, linked by the dimensionless shear rate $\chi^+ = a\chi/V$ and the dimensionless angular velocity $\omega^+ = a\omega/V$), the dimensionless force exerted by the fluid on the sphere, obtained by dividing the actual force by $\frac{1}{2}\rho V^2 \pi a^2$, is computed by integrating the viscous and pressure stresses over the surface of the sphere:

$$\mathbf{F}^+ = \frac{4}{\pi}\int_{\theta=0}^{\theta=\pi}\int_{\phi=0}^{\phi=\pi}\left(\tau^{=} - p\delta^{=}\right)\mathbf{n} r \sin\theta \, \mathrm{d}\theta \, \mathrm{d}\phi \qquad [26]$$

taking into account that on the sphere surface, $r = 1$, $\partial u/\partial\phi = 0$ and $\partial u/\partial\theta = 0$. The drag and lift coefficients, which correspond, respectively, to the z- and x-directions, are given by:

$$C_D = \frac{4}{\pi}\int_{\theta=0}^{\theta=\pi}\int_{\phi=0}^{\phi=\pi}\left[\left(\frac{2}{Re_p}\frac{\partial u}{\partial r} - p\right)\cos\theta - \frac{1}{Re_p}\frac{\partial}{\partial r}\left(\frac{v}{r}\right)\sin\theta\right]\sin\theta \, \mathrm{d}\theta \, \mathrm{d}\phi, \qquad [27]$$

$$C_L = \frac{4}{\pi}\int_{\theta=0}^{\theta=\pi}\int_{\phi=0}^{\phi=\pi}\left[\left(\frac{2}{Re_p}\frac{\partial u}{\partial r} - p\right)\sin\theta\cos\phi + \frac{1}{Re_p}\left(\frac{\partial}{\partial r}\left(\frac{v}{r}\right)\cos\theta\cos\phi - \frac{\partial}{\partial r}\left(\frac{w}{r}\right)\sin\phi\right)\right] \times \sin\theta \, \mathrm{d}\theta \, \mathrm{d}\phi. \qquad [28]$$

The torque experienced by the sphere, which is directed by $\mathbf{j}$, is computed by integrating the moment, at the centre of the sphere, of the viscous surface forces. As for the lift and drag forces, $\partial u/\partial\theta = \partial u/\partial\phi = 0$ for $r = 1$, so that the following expression is finally obtained, where the torque is non-dimensionalized by $1/2\rho V^2\pi a^3$:

$$C_T = -\frac{4}{\pi Re_p}\int_{\theta=0}^{\theta=\pi}\int_{\phi=0}^{\phi=\pi}\left[\frac{\partial}{\partial r}\left(\frac{w}{r}\right)\cos\theta\sin\phi - \frac{\partial}{\partial r}\left(\frac{v}{r}\right)\cos\phi\right]\sin\theta \, \mathrm{d}\theta \, \mathrm{d}\phi. \qquad [29]$$

4. RESULTS AND DISCUSSION

4.1. *Accuracy and grid sensitivity*

The accuracy of the numerical technique used here was tested by comparing the computed flow pattern, as well as the drag, lift and torque coefficients, with available results in specific flow configurations. In addition, grid checks have been carried out in order to study the influence of the number of grid points and of the location of the outer boundary.

Table 1. Comparison between theoretical and computed values of C_L, C_D and C_T at $Re_p = 5 \times 10^{-4}$, $\omega^+ = 1$ and $\chi^+ = 0$

Grid parameters				Theoretical coefficients			Computed coefficients		
h	n_i	$n_j = n_k$	r_{max}	C_L	C_D	C_T	C_L	C_D	C_T
0.12	50	20	358	−2	24 004	−32 000	−2.05	24 676	−31 872
0.1	58	22	299	−2	24 004	−32 000	−2.04	24 641	−31 870

At small Reynolds numbers, our results were compared with the theoretical ones according to Rubinow and Keller (1961) for a spinning sphere in a uniform flow and given by the following relationships:

$$C_D = \frac{12}{Re_p}\left(1 + \frac{3}{8}Re_p\right), \quad [30]$$

$$C_L = -2\omega^+(1 + O(Re_p)), \quad [31]$$

$$C_T = -\frac{16\omega^+}{Re_p}(1 + o(Re_p)), \quad [32]$$

where ω^+ is the dimensionless angular velocity defined by $\omega^+ = a\omega/V$.

Examples of numerical results, as shown by table 1 for $Re_p = 5 \times 10^{-4}$, $\omega^+ = 1$ and $\chi^+ = 0$, can be seen to be very satisfactory for such low Reynolds number flow cases: lift and drag are predicted within 2–3% and the torque value is obtained with an accuracy of 0.4%. Morever, it can be observed that the location of the outer boundary (radius r_{max}) and the grid parameters have a very slight influence on the computed coefficients. Manipulating the grid spacing in the angular directions has only a little effect on the values of the lift, drag and torque coefficients. It should be mentioned, however, that a very large value of r_{max} is needed for such a low Reynolds number. At higher Reynolds number, this value may be reduced without loss of accuracy.

At moderate Reynolds numbers, the accuracy of the numerical method is checked through comparison with the available results in the literature for the case of a non-rotating sphere in a steady uniform flow. For this purpose, drag coefficients are computed at $\omega^+ = 0$ for Reynolds numbers between 0.1 and 20 and compared with the values yielded by the correlation of Morsi and Alexander (1972), which gives the best available fit with standard curve values. The result of such a comparison is illustrated by figure 2. A very good agreement can be observed between

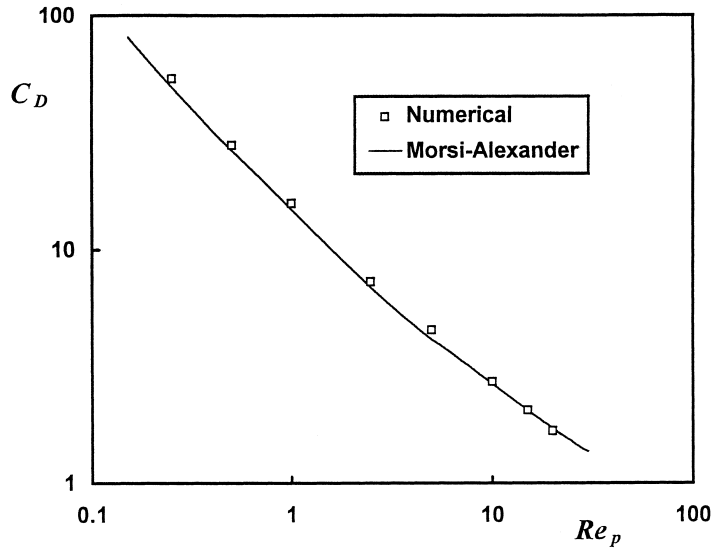

Figure 2. A comparison between the predicted drag coefficients (symbols) and the values taken from the correlation of Morsi and Alexander (1972) (solid line).

the numerically calculated drag coefficients and the experimental ones. In addition, properties of the recirculation wake, such as the separation Reynolds number and the wake length, can be compared with published results. Taneda (1956) observed the phenomenon of separation at $Re_p = 12$. Measurements by Payard and Coutanceau (1974), however, do not agree with Taneda's result since they found that a wake existed behind the sphere as soon as $Re_p = 8.5$. Another result concerning the recirculation wake is given by Dennis and Walker (1971), who obtained numerically a separation for $Re_p \cong 10$. In the present study, the separation was detected for $10 \leq Re_p \leq 12$, in good agreement with the results of Taneda (1956) and Dennis and Walker (1971). Figure 3 shows the computed velocity field and streamline pattern for

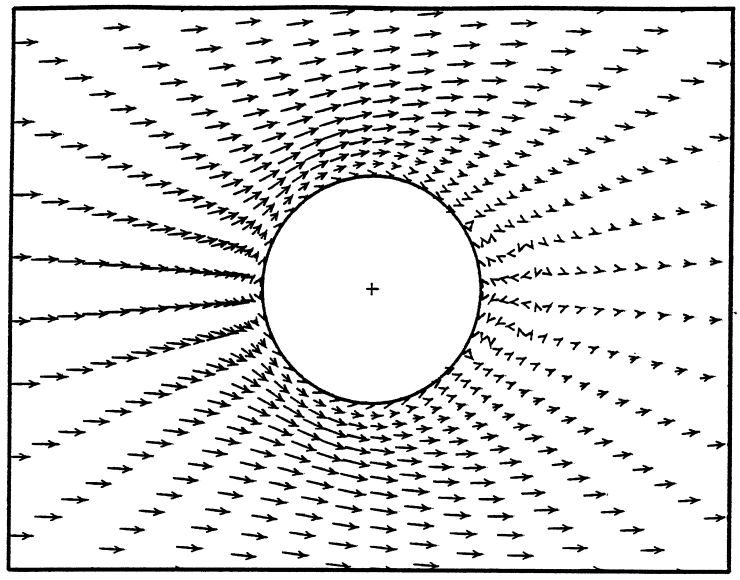

(a)

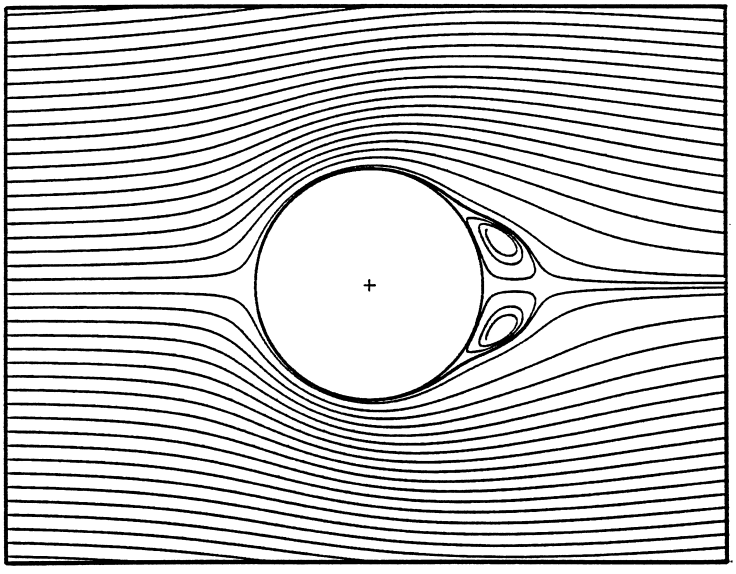

(b)

Figure 3. Flow field at $Re_p = 20$ and $Re_\omega = Re_\chi = 0$: (a) velocity field; (b) streamlines.

Table 2. Influence of outer boundary location and grid density on C_L, C_D and C_T at $Re_p = 5 \times 10^{-4}$, $\omega^+ = 0$ and $\chi^+ = 0.1$

n_i	$n_j = n_k$	h	r_{max}	C_L	C_D	C_T
48	20	0.09	69	24.6	25 142	−1672
48	20	0.1	110	56	24 920	−1673
53	20	0.09	110	54.3	24 870	−1673
68	20	0.07	110	55.6	24 750	−1673
48	22	0.1	110	55.5	24 925	−1671
48	24	0.1	110	55.2	24 930	−1669
56	24	0.1	244	39	24 773	−1679
		Theoretical values→		58.2	24 005	−1600

$Re_p = 20$. The corresponding predicted eddy length is 0.56 radii. This value lies between the estimations of Payard and Coutanceau (1974) and Dennis and Walker (1971), who obtained, respectively, 0.5 and 0.6 radii at the same Reynolds number.

In case of a linear shear flow, the numerical results can be compared with the theoretical ones under the conditions of Saffman (1965, 1968) or McLaughlin (1991). As shown by table 2, which provides an illustration of the influence of both the outer boudary location and the grid density on the computed values of C_L, C_D and C_T, for $Re_p = 5 \times 10^{-4}$ and $\chi^+ = 0.1$, the lift coefficient can be seen to be strongly influenced by the outer radius r_{max}, thus making it difficult to obtain reliable lift predictions when shear is present.

However, for such a small value of Re_p, better results would have been expected in increasing the radius of the computational domain since the Oseen region, whose radius is $O(Re_p^{-1})$, extends to $r_{max} \approx 2000$. Unfortunately, larger values of r_{max} were found to unavoidably lead to numerical divergence, presumably because of the very high (and physically meaningless) outer boundary velocity, whose dimensionless value reaches $1 + \chi^+ r_{max}$ on the x-axis. By choosing a higher value of the Reynolds number in order to reduce the Oseen radius, the same problem arises since we have to select a higher value of χ^+ for the Saffman conditions to be met. This has been confirmed by further tests performed at $Re_p = 5{\cdot}10^{-2}$, for which a value of χ^+ of order of 1 is needed: in this case, no convergence could be obtained for $r_{max} > 27$ and the predicted lift coefficient was still very sensitive to the outer boundary location. Such a grid sensitivity for the lift coefficient was also mentioned by Dandy and Dwyer (1990). On the contrary, the computed torque and drag coefficients appear to be negligibly influenced by the choice of the outer boundary radius and grid parameters, although they are slightly overestimated (about 4%).

Nevertheless, it must be mentioned that the influence of the grid parameters on the velocity and pressure fields is not noticeable, as can be seen in figures 4 and 5, which display the velocity field, streamline pattern and pressure field obtained for two different grids and for the same values of Re_p and χ^+. The influence of the grid parameters has also been tested at higher Reynolds numbers. Although satisfactory results were obtained in uniform flow, it was found that the lift coefficient is significantly affected by the grid parameters as soon as shear flow is considered. The torque coefficient and the flow pattern, however, are not observed to be influenced by the grid parameters.

From these preliminary tests, it may be concluded that the present study can provide reliable results regarding the flow pattern and the torque coefficient. In addition, some information about the combined effects of shear and spin on the lift and drag coefficients, at small Reynolds numbers, will be given in adopting, for each value of the shear Reynolds number Re_χ, the grid parameters which led to the best agreement with the theoretical lift at $\omega^+ = 0$ according to McLaughlin (1991).

4.2. *Flow pattern*

It may be interesting to examine the modifications induced in the flow structure by the sphere rotation and by the shear. The typical value of the particle Reynolds number considered here is $Re_p = 20$ and the dimensionless shear rates are $\chi^+ = 0.025$, $\chi^+ = 0.05$ and $\chi^+ = 0.20$. Velocity fields, stream lines and pressure fields in the symmetry plane, which is orthogonal to the rotation axis, are plotted in figures 6–10. Streamlines were obtained by numerically following the trajec-

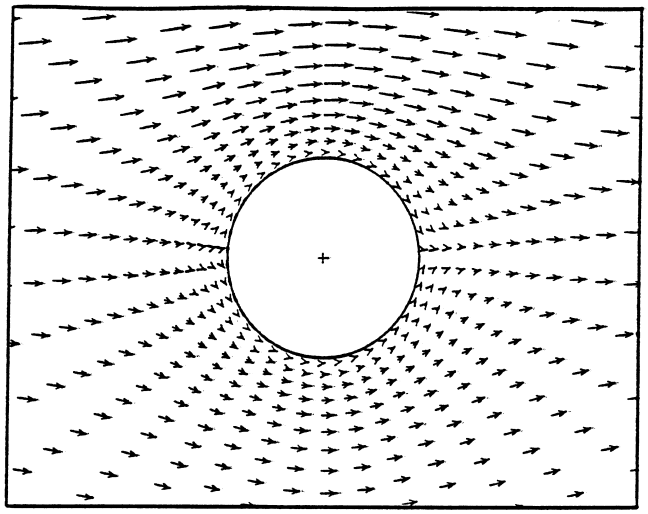

(a)

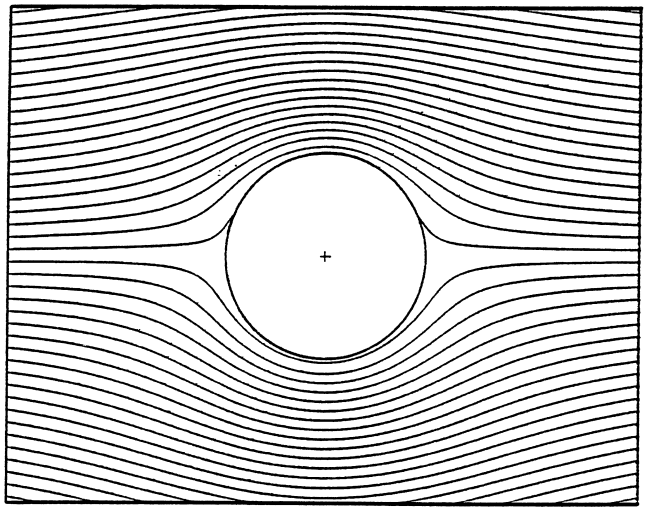

(b)

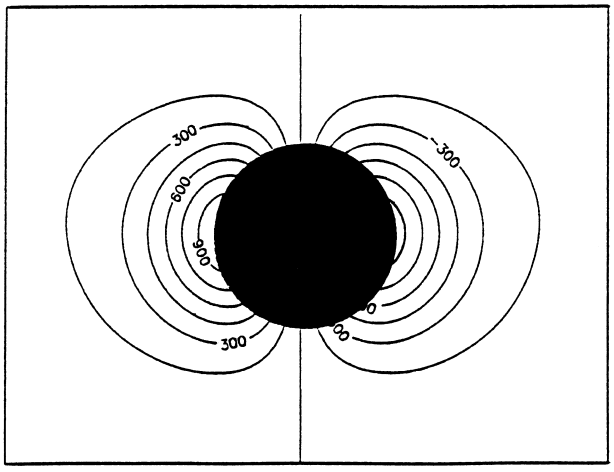

(c)

Figure 4. Flow pattern, in the symmetry plane x–z, at $Re_p = 5 \times 10^{-4}$, $Re_\omega = 0$ and $Re_\chi = 5 \times 10^{-5}$ ($\chi^+ = 0.1$). Grid parameters: $n_i = 48$, $n_j = 20$, $n_k = 20$, $r_{max} = 110$. (a) Velocity field; (b) streamlines; (c) pressure field (numbers refer to the values of the dimensionless pressure).

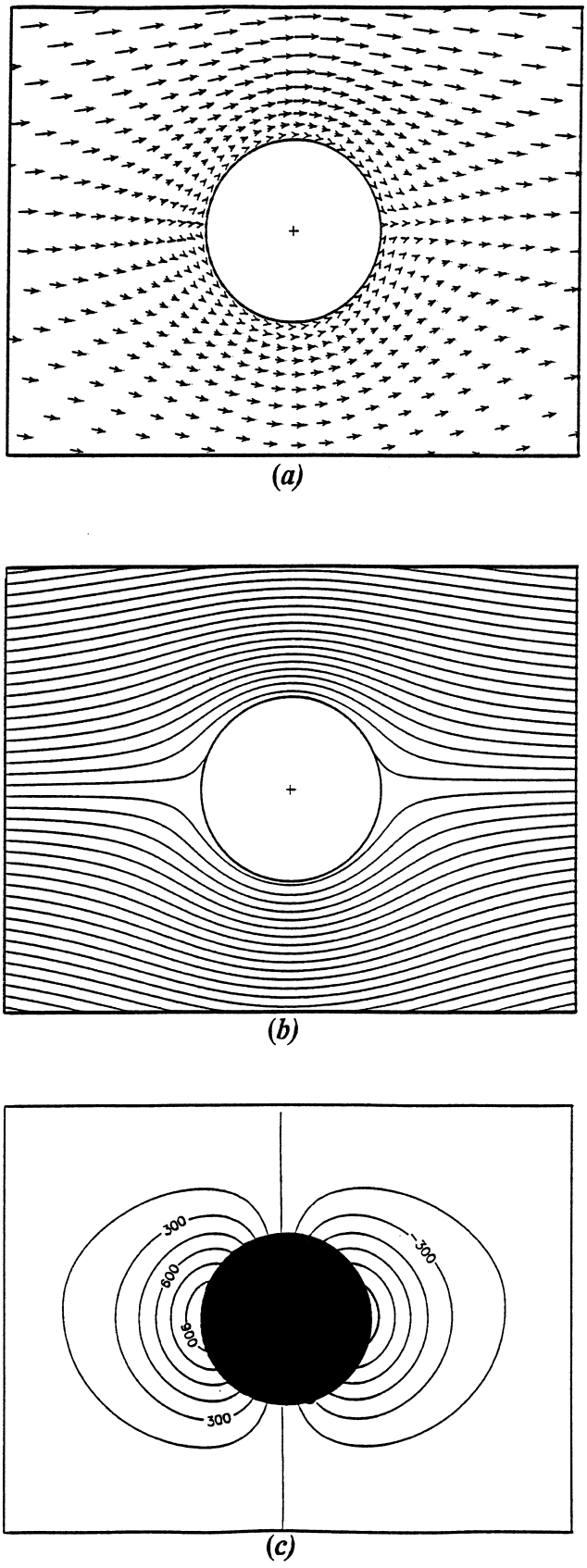

Figure 5. Flow pattern, in the symmetry plane x–z, at $Re_p = 5 \times 10^{-4}$, $Re_\omega = 0$ and $Re_\chi = 5 \times 10^{-5}$ ($\chi^+ = 0.1$). Grid parameters: $n_i = 56$, $n_j = 24$, $n_k = 24$, $r_{max} = 244$. (a) Velocity field; (b) streamlines; (c) pressure field (numbers refer to the values of the dimensionless pressure).

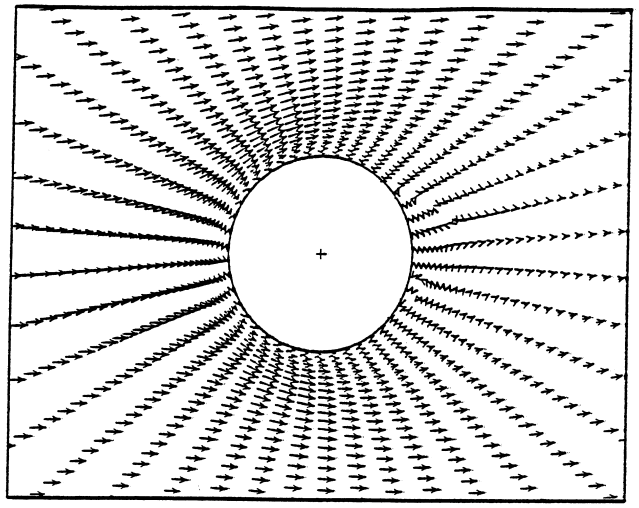

(a)

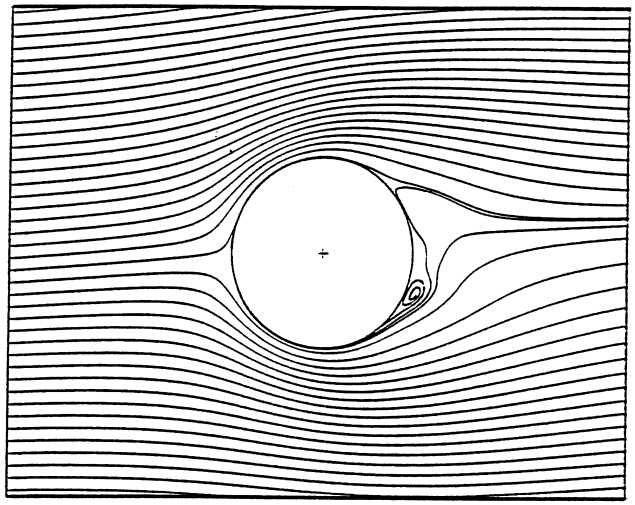

(b)

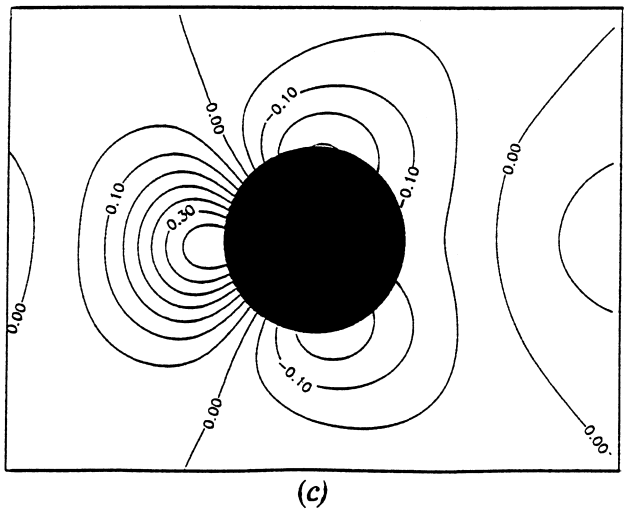

(c)

Figure 6. Flow pattern, in the symmetry plane x–z, for $Re_p = 20$, $\chi^+ = 0.025$ and $\omega^+ = 0$: (a) velocity field; (b) streamlines; (c) pressure field (numbers refer to the values of the dimensionless pressure).

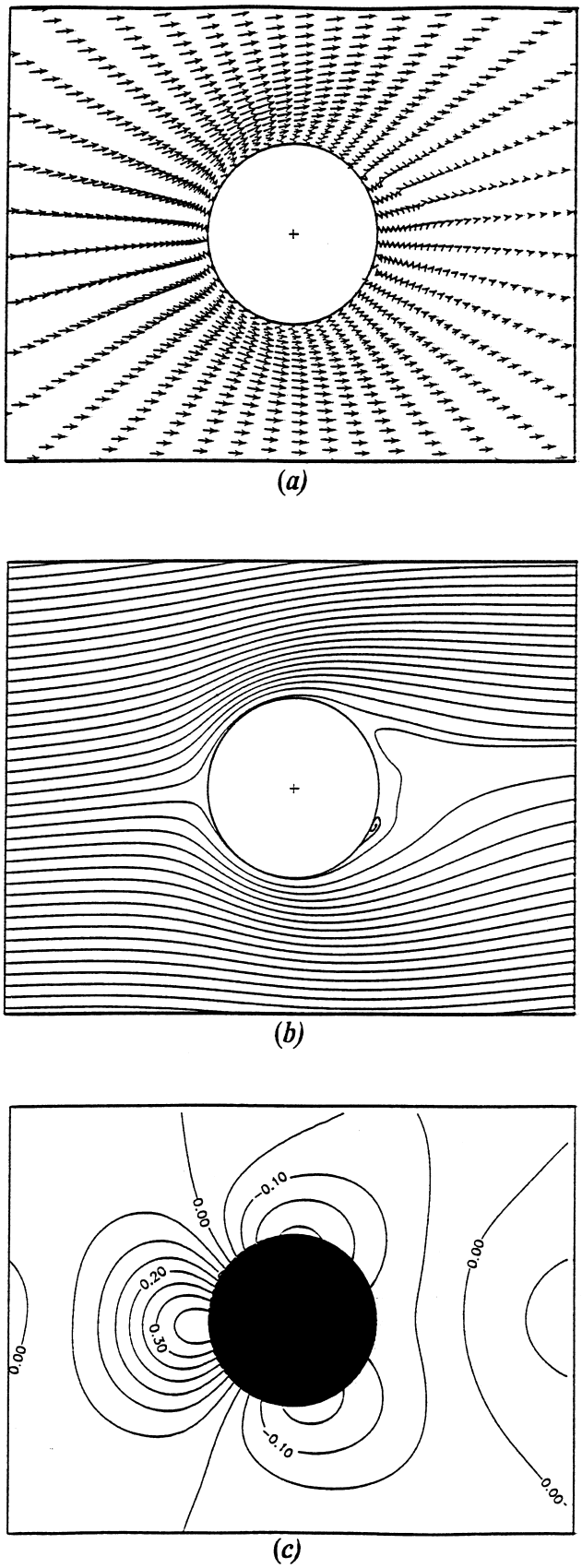

Figure 7. Flow pattern, in the symmetry plane x–z, for $Re_p = 20$, $\chi^+ = 0.05$ and $\omega^+ = 0$: (a) velocity field; (b) streamlines; (c) pressure field (numbers refer to the values of the dimensionless pressure).

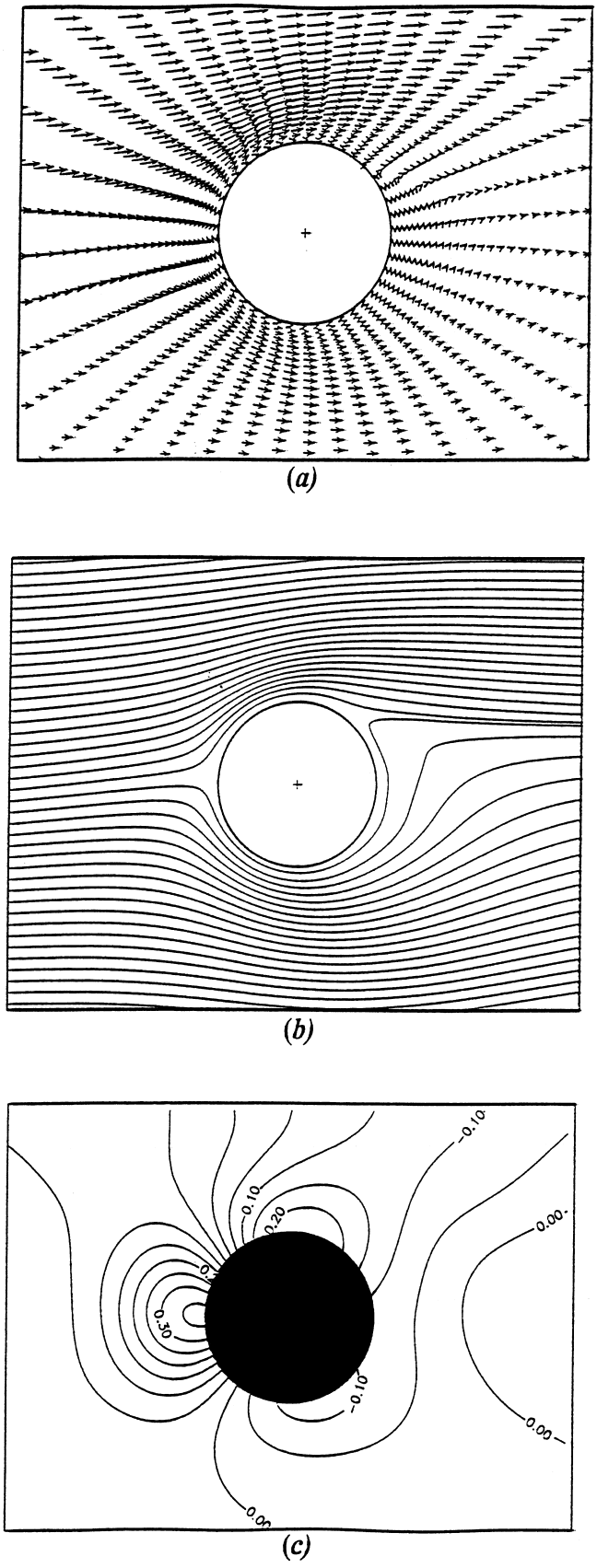

Figure 8. Flow pattern, in the symmetry plane x–z, for $Re_p = 20$, $\chi^+ = 0.20$ and $\omega^+ = 0$: (a) velocity field; (b) streamlines; (c) pressure field (numbers refer to the values of the dimensionless pressure).

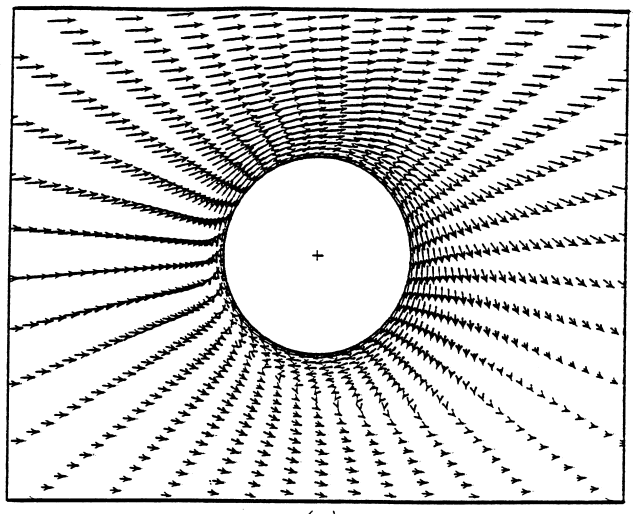

(a)

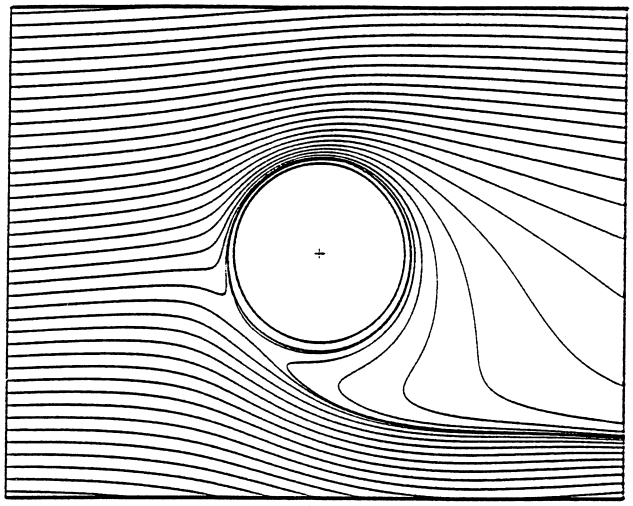

(b)

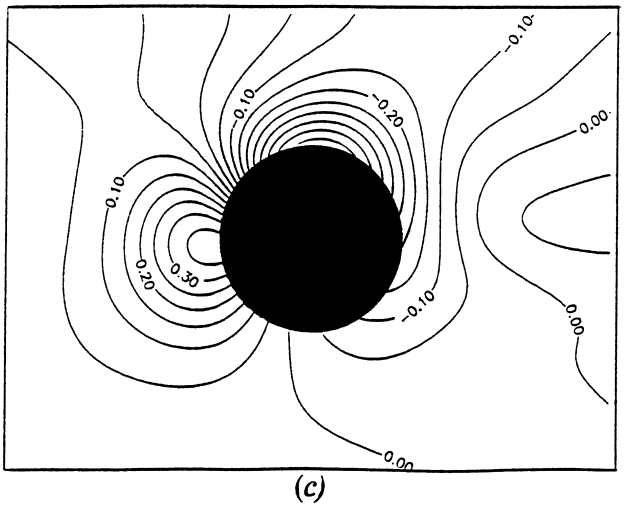

(c)

Figure 9. Flow pattern, in the symmetry plane x–z, for $Re_p = 20$, $\chi^+ = 0.20$ and $\omega^+ = -1$: (a) velocity field; (b) streamlines; (c) pressure field (numbers refer to the values of the dimensionless pressure).

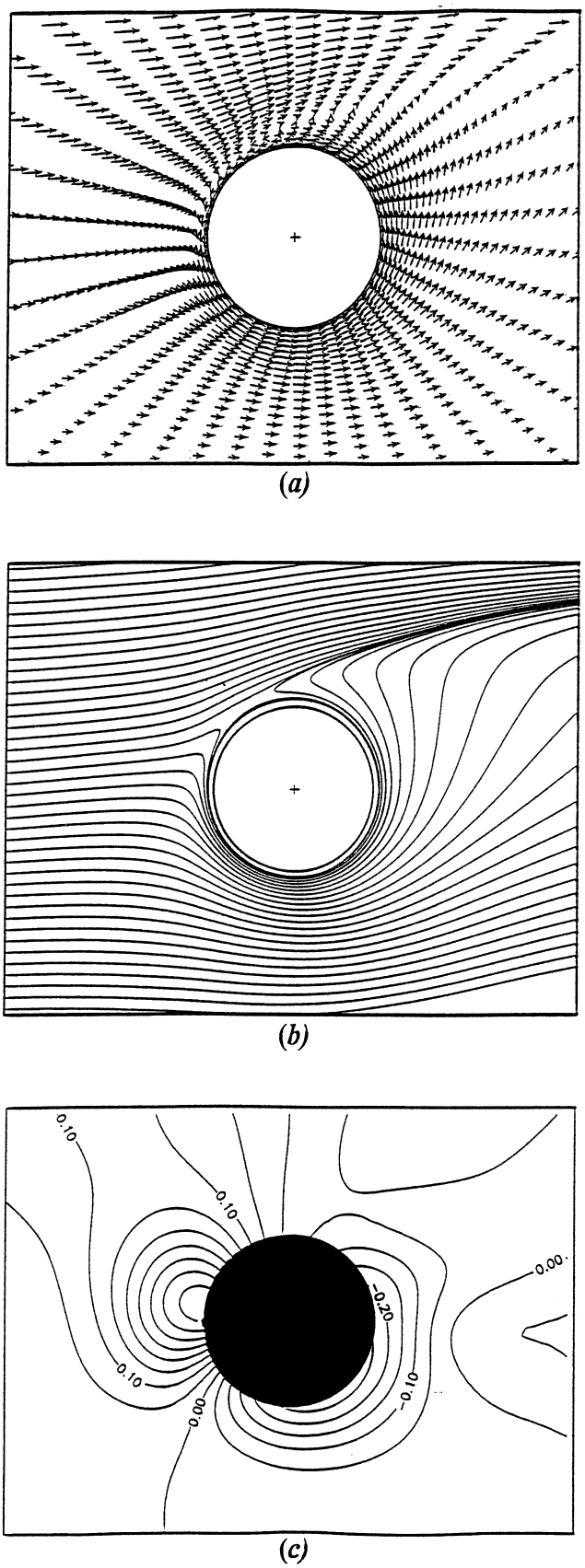

Figure 10. Flow pattern, in the symmetry plane x–z, for $Re_p = 20$, $\chi^+ = 0.20$ and $\omega^+ = +1$: (a) velocity field; (b) streamlines; (c) pressure field (numbers refer to the values of the dimensionless pressure).

tories of equally spaced tracers upstream of the sphere and additional trajectories have been computed in order to visualize the recirculation when necessary.

In order to examine the influence of shear in the absence of spin, figures 6–8 may be compared with figure 3. At low shear rates, as shown by figures 6 and 7, the forward stagnation point is slightly shifted towards the low-velocity side and closed streamlines exist at the rear of the sphere. However, even though a separation still takes place on the upper surface, the upper recirculating eddy has disappeared. The size of the remaining eddy is seen to decrease with increasing shear rate (figures 6 and 7), until it vanishes completely, for a value of χ^+ comprised between 0.05 and 0.1. At higher shear rate, as illustrated by figure 8 ($\chi^+ = 0.20$), the upstream stagnation point is slightly displaced towards the high-velocity side and there is now only one separation point (in the symmetry plane) at the rear of the sphere, which is located on the upper portion of the sphere surface. Such observations are very similar to the behaviour reported by Dandy and Dwyer (1990) for a higher value of the Reynolds number ($Re_p = 35$). In this case, the recirculating eddy was found by these authors to be shifted towards the low-velocity side of the sphere for low values of the shear rate and to disappear for $\chi^+ > 0.2$.

Owing to the velocity gradient of the undisturbed flow, the velocity is seen to significantly increase from the bottom to the top of the figure, leading to larger wall shear stresses on the upper side of the sphere, which undergoes therefore a torque in the clockwise direction. The asymmetry due to the shear has obviously consequences for the pressure field: figure 8(c) shows that the pressure is lower on the top of the sphere, where the velocity is higher, as could be expected. Besides the resulting lift force, the modified pressure and shear stress distributions may possibly alter the drag force.

In case of sphere rotation, there is only one stagnation point, the location of which is displaced at a distance of the sphere surface, due to the no-slip condition which leads to the presence of a rotating layer close to the sphere surface. This can be seen in examining the streamlines in figures 9 and 10, which refer to opposite rotation directions. In figure 9, the fluid motion is enhanced by the peripheral velocity in the upper region of the flow, so that the stagnation point is located on the low velocity side of the fluid flow. This leads to a strong decrease of the pressure on the top of the sphere, as shown by figure 9(c). On the contrary, the stagnation point is located in the upper region of the flow when ω^+ is positive (figure 10) and in this case the minimal pressure is not so low as in the previous case, as can be observed in figure 10(c). In both cases, the angular velocity may be expected to have an important influence on the torque, owing to the high shear stress produced at the sphere surface by the rotational motion.

4.3. *Lift and drag at small Reynolds number*

An example of results concerning the lift coefficient at small Reynolds numbers is displayed in figure 11, where C_L is plotted as a function of the shear Reynolds number Re_χ, for several values of the dimensionless angular velocity ω^+, at a fixed value of the particle Reynolds number, namely $Re_p = 0.05$. The theoretical results of Saffman (1965, 1968) and McLaughlin (1991) for $\omega^+ = 0$ are also plotted in this figure, in order that the corresponding computed lift coefficients can be compared with the theoretical ones. It must be pointed out that Saffman's conditions, given by [1], are not satisfied in the range of Reynolds numbers and dimensionless shear rates investigated here, thereby the only valid theoretical result is Mclaughlin's one, with which the numerically predicted lift coefficients at $\omega^+ = 0$ can be observed to be in very close agreement. Furthermore, it may be noted that the values of C_L in uniform flow (Re_χ) are in accordance with the theoretical result of Rubinow and Keller (1961), namely $C_L = 2\omega^+$. Results regarding the lift of a spinning sphere in uniform flow at higher Reynolds numbers will be presented and discussed in a forthcoming paper.

Although the lift is known to arise from inertia effects, i.e. from the non-linear behaviour of the equations of motion, figure 11 shows that a good approximation is provided by adding the theoretical lift of a fixed sphere in a shear flow (according to McLaughlin 1991) and the theoretical lift of a spinning sphere placed in a uniform flow (Rubinow and Keller 1961). This can be explained by the fact that the inertial terms are nevertheless very small compared with the viscous ones for such low Reynolds numbers. As a consequence, it can be concluded that the lift

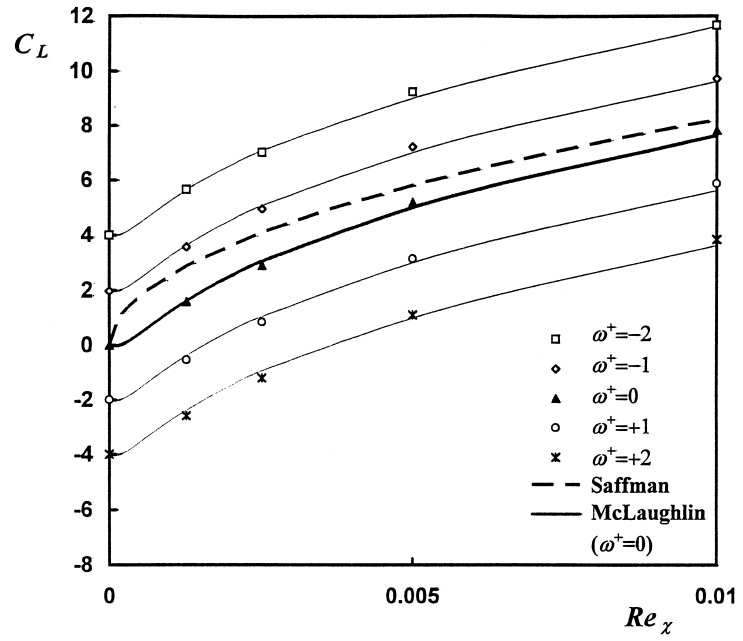

Figure 11. A plot of the lift coefficient at $Re_p = 0.05$ as a function of the shear Reynolds number Re_χ for several values of ω^+. The thin solid lines are obtained by adding the theoretical solutions of McLaughlin (1991) and of Rubinow and Keller (1961).

force on a spinning sphere in a linear shear flow can be obtained by superposing McLaughlin's results and Rubinow and Keller's results, provided that the characteristic Reynolds numbers be small enough.

Results regarding the drag coefficient at small Re_p are represented in figure 12, which is a plot of the ratio C_D/C_{DO} (C_{DO} being the Oseen's drag coefficient for uniform flow) as a function of ω^+ for several values of the dimensionless shear rate χ^+. It can be seen that the drag is slightly increasing with increasing shear rate, as has already been observed by Yamamoto *et al.* (1993), who studied the lift and drag applied to a sphere in a high Reynolds number linear shear flow.

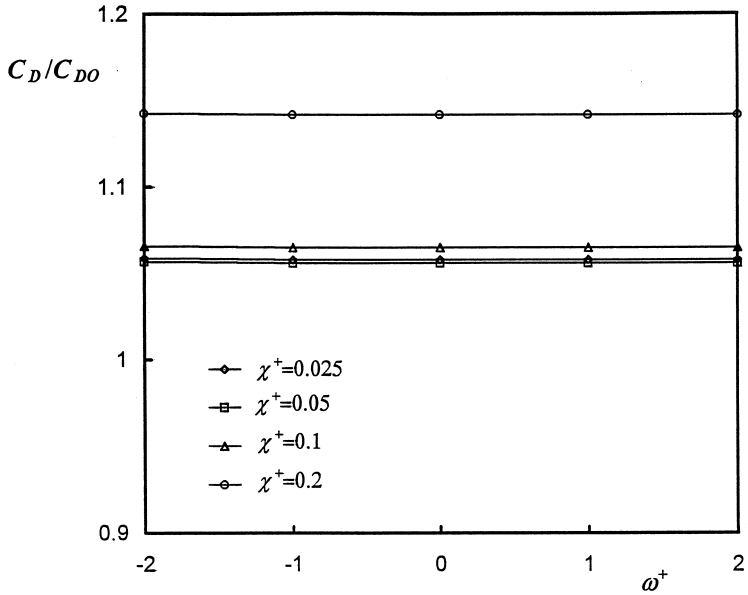

Figure 12. The ratio C_D/C_{DO} as a function of ω^+ at $Re_p = 0.05$, for several values of χ^+ (C_{D0} is the Oseen's drag coefficient for uniform flow).

It is also interesting to note that the drag is not altered by the rotation of the sphere at such low Reynolds numbers.

4.4. *Torque*

The results reported here relate to the torque coefficient C_T, which was found to be insensitive to the grid parameters and which was not studied, under the influence of both shear and spin, by any author yet. At first, let us examine the influence of both spin and shear on the torque coefficient at small values of the sphere Reynolds numbers. Examples of results obtained at $\omega^+ = 1$, $Re_p = Re_\omega = 0.05$ and $Re_p = Re_\omega = 0.5$, are presented in figure 13, which displays the ratio C_T/C_{TO} as a function of χ^+ (C_{TO} being the torque coefficient at $\chi^+ = 0$). The theoretical analysis of Rubinow and Keller 1961) is valid for such low values of Reynolds numbers Re_p and Re_ω, provided that $\chi^+ = 0$ (uniform flow). In the case $\chi^+ \neq 0$, some authors used the Rubinow and Keller's relationship in replacing the sphere angular velocity ω by $\omega + \chi/2$, which is the relative angular velocity with respect to the fluid rotation velocity. It can be seen from figure 13 that such a simplification, which is only valid under creeping flow conditions, as shown by Faxen, leads to a slight underestimation of the torque coefficient. Let us recall that Faxen's formula may be written as follows:

$$C_{T(\text{Faxen})} = -\frac{16}{Re_p}\left(\omega^+ + \frac{\chi^+}{2}\right), \qquad [33]$$

Before presenting the effect of simultaneous shear and rotation at moderate Reynolds numbers Re_p, ranging up to 20, it is more useful to examine first the numerical results concerning the shear induced torque coefficient, i.e. without spin. In this case, the Faxen's formula [33] shows that the dimensionless torque under creeping flow conditions is proportional to the dimensionless shear rate and inversely proportional to the sphere Reynolds number. In order to study the influence of both parameters Re_p and χ^+ at higher Reynolds numbers, the computed values of the ratio $C_{T(\omega=0)}/\chi^+$ are plotted, in figure 14, as a function of Re_p and are compared with the theoretical result of Faxen given by [33]. It can be seen that Faxen's formula underestimates the torque coefficient in the range of Reynolds numbers investigated herein ($Re_p \geq 0.5$) and that the ratio $C_{T(\omega=0)}/\chi^+$ is depending on χ^+, even at $Re_p = 0.5$. The deviation from low Reynolds number theory is found to be significantly increasing for $Re_p \geq 10$. As shown by figure 15, such a behaviour may be depicted by the following modified expression of the torque coefficient, which is a correlation of the present numerical results:

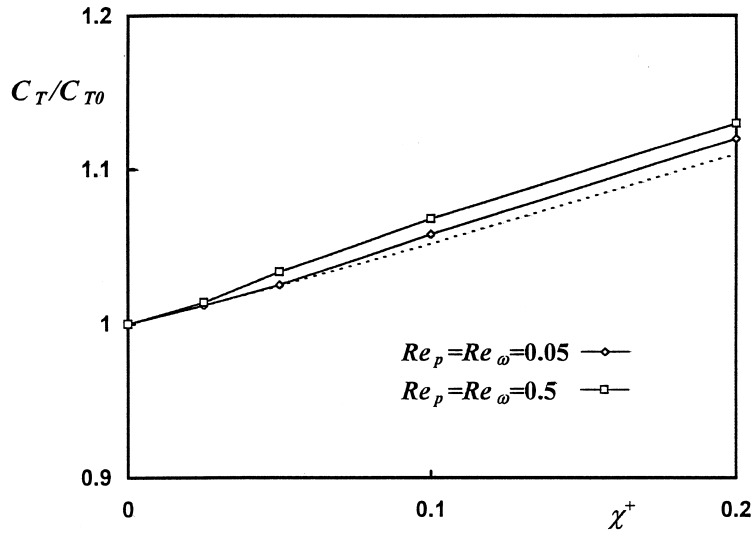

Figure 13. The torque coefficient as a function of χ^+ for small Reynolds numbers ($\omega^+ = 1$). The dotted line refers to the torque obtained by replacing the absolute sphere angular velocity ω by the relative velocity $\omega + \chi/2$ in the formula of Rubinow and Keller.

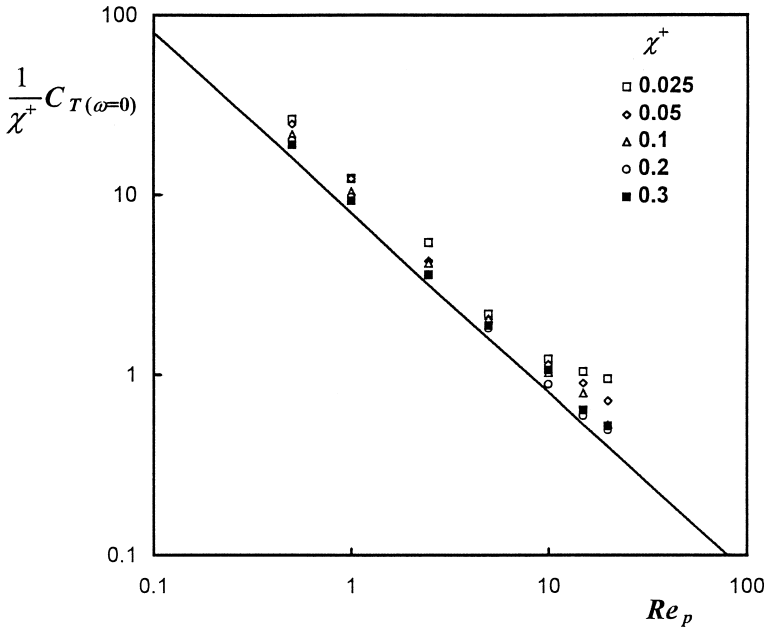

Figure 14. Predicted values of the torque coefficient in case of zero angular velocity, illustrated by the ratio C_T/χ^+ as a function of Re_p for several values of the dimensionless shear rate χ^+. The solid line refers to Faxen's formula [33].

$$C_{T(\omega=0)} = -\frac{8}{Re_p}(\chi^+)^{0.9}\left(1 + 1.3 \times 10^{-4} Re_p^2 (\chi^+)^{-0.7}\right). \quad [34]$$

The relative torque increment $(\Delta C_T/C_T)_{(\omega=0)}$, where ΔC_T is defined by $\Delta C_T = C_T - C_{T(Faxen)}$, may reach very high values at low shear rate. In the present calculations, the maximum deviation from Faxen's formula, obtained for $Re_p = 20$ and $\chi^+ = 0.025$, is $(\Delta C_T/C_T)_{(\omega=0)} = 137\%$. Although there is no evidence of connection between such a notable inertia effect and the

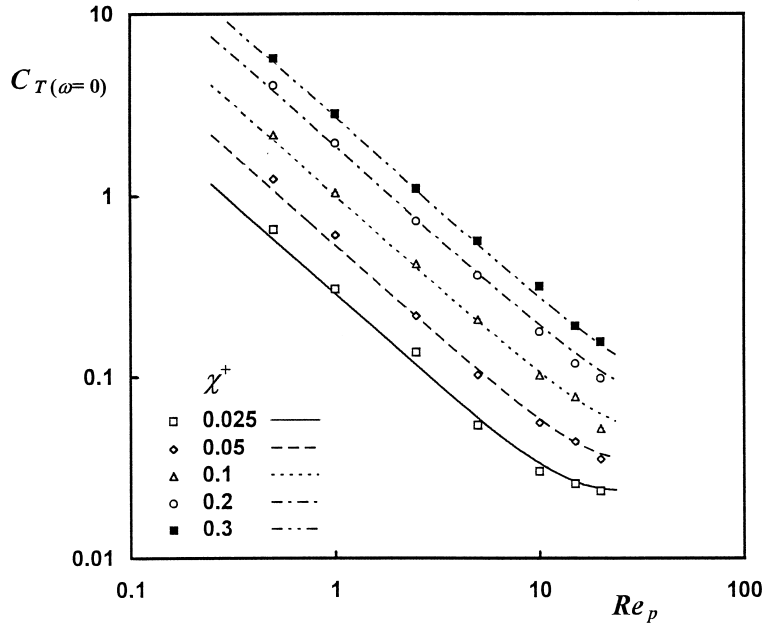

Figure 15. Comparison between the proposed correlation [[34], represented by lines] and the computed values (marks) of the shear induced torque coefficient $C_{T(\omega=0)}$.

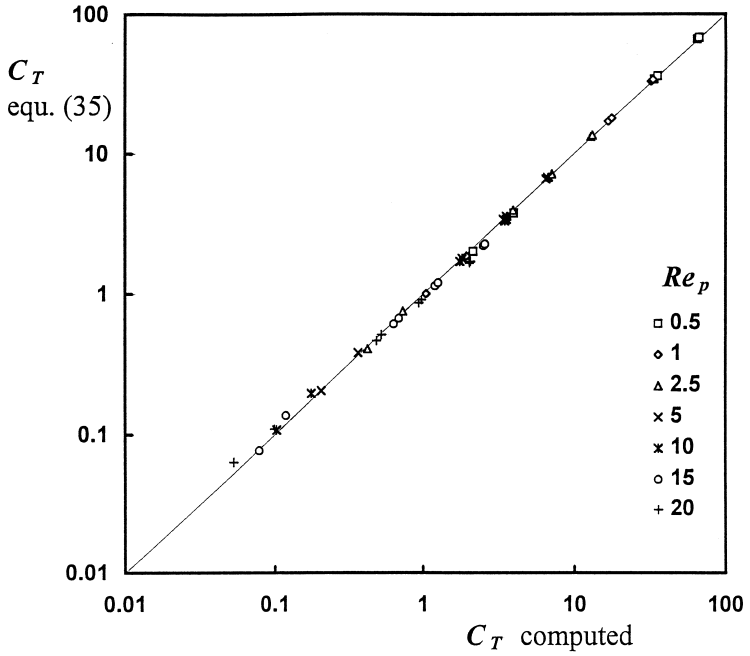

Figure 16. Illustration of [35].

observed flow pattern, a possible explanation of the torque increase at low shear rate lies in the upper eddy disappearing, which leads to a decrease of the influence of the wall shear stress on the lower portion of the sphere surface.

In case of a spinning sphere, it may be mentioned first that the torque due to spin in a uniform flow ($\chi^+ = 0$) was found to agree well with the theoretical finding of Rubinow and Keller [32] in the range of Re_ω investigated herein. This means that the spin induced torque seems to be much less sensitive to inertia effects than the shear induced torque. In the presence of both shear and spin, the torque coefficient was computed for several values of ω^+ and χ^+, in the ranges $-2 \leq \omega^+ \leq +2$ and $0 \leq \chi^+ \leq +0.3$. The corresponding ranges of the shear and rotation Reynolds numbers are $Re_\chi \leq 6$ and $Re_\omega \leq 40$. In spite of the moderately high values of the particle Reynolds numbers, implying that the inertial terms in the equations of motion are no longer negligible, it was observed that the torque coefficient C_T could be approximated by adding the torque coefficient due to the spinning motion of the sphere in a uniform flow and the shear induced torque coefficient without spin as given by the above proposed correlation [34]. As a consequence, the following correlation, obtained by adding the torque coefficient expressions [32] and [34], is finally proposed:

$$C_T = -\frac{16}{Re_p}\left(\omega^+ + \frac{1}{2}(\chi^+)^{0.9} + 6.5 \times 10^{-5} Re_p^2 (\chi^+)^{0.2}\right). \quad [35]$$

This result can easily be extended to negative shear rates in the range $-0.3 \leq \chi^+ \leq 0$, in replacing χ^+ by $|\chi^+|$ and changing the sign of the two last terms. An illustration of the proposed correlation, which is valid in the aforementioned ranges of flow parameters, is provided by figure 16, where the numerically computed torque coefficients are plotted versus the correlated values of C_T according to [35], for several values of particle Reynolds number, dimensionless shear rate and dimensionless angular velocity. [35] can be seen to adequately describe the numerically predicted torque in a range of finite Reynolds numbers, $0.5 \leq Re_p \leq 20$, which are frequently encountered in gas–solid or liquid–solid two-phase flows.

5. CONCLUSION

Numerical solutions have been obtained for the steady linear shear flow past a rotating sphere in the range of particle Reynolds numbers based on sphere radius $Re_p \leq 20$, dimensionless shear

rates $-0.3 \leq \chi^+ \leq 0.3$ and dimensionless angular velocities $-2 \leq \omega^+ \leq +2$. The full Navier–Stokes equations have been solved using a finite volume formulation based on a pressure correction procedure. Original results concerning the flow pattern, the lift and drag forces and mainly the torque, which was not studied by any author yet, have been presented.

Examination of the flow pattern has shown an important effect of the shear at the rear of the sphere. In particular, in the absence of rotation, at $Re_p = 20$, the recirculating region, which is known to exist in a uniform flow, has been found to be significantly reduced at low shear rate and to vanish for $\chi^+ \geq 0.1$. The recirculating eddy also disappears in case of sphere rotation, due to the no-slip condition, which leads to the presence of a rotating layer close to the sphere surface.

The lift and the drag coefficients were found to be significantly sensitive to the grid parameters in case of shear flow, so that reported results have been restricted to small Reynolds numbers. In this case the lift is found to be the sum of McLaughlin's shear induced lift and of Rubinow and Keller's spin induced lift, whereas the drag is slightly increased by the velocity gradient, but is not affected by the rotation of the sphere. It has also been shown that replacing the angular velocity ω by the relative angular velocity $\omega + \chi/2$ in the Rubinow and Keller's result leads to a slight underestimation of the torque.

Results concerning the torque coefficient, which was shown not to be influenced by the grid parameters, have been extended to higher particle Reynolds numbers. For Re_p ranging from 0.5 to 20, the torque due to shear has been found to be notably increased by inertia effects, compared with the theoretical torque at small Reynolds numbers given by Faxen's formula. This may be due to the significant displacement of the downstream stagnation point towards the larger velocity side of the sphere. Inertia effects upon the spin induced torque in uniform flow seem to be much lower, so that the result of Rubinow and Keller (1961) may still be used for $\chi^+ = 0$. In the case of simultaneous influences of shear and spin, the torque coefficient was finally found to obey the following correlation, provided that $Re_p \leq 20$, $-0.3 \leq \chi^+ \leq 0.3$ and $-2 \leq \omega^+ \leq +2$:

$$C_T = -\frac{16}{Re_p}\left(\omega^+ \pm \frac{1}{2}|\chi^+|^{0.9} \pm 6.5 \times 10^{-5} Re_p^2 |\chi^+|^{0.2}\right)$$

where the plus signs are for positive χ^+ and the minus signs for negative χ^+.

Although further improvements of the numerical code are needed in order to achieve more reliable predictions of the lift and drag coefficients, the proposed correlation may be helpful for the computation of solid particle trajectories in confined flows, where both particle spin and fluid shear have to be taken into account.

REFERENCES

Auton, T. R. (1987) The lift force on a spherical body in a rotational flow. *Journal of Fluid Mechanics* **183,** 199–218.

Bretherton, F. P. (1962) The motion of rigid particles in a shear flow at low Reynolds number. *Journal of Fluid Mechanics* **14,** 284–304.

Chegroun, N. (1992) Etude numérique des actions hydrodynamiques sur une sphère en translation et rotation dans la gamme des nombres de Reynolds inférieurs à 50. Thèse de l'Institut National Polytechnique de Lorraine, Nancy, France.

Cherukat, P., McLaughlin, J. B. and Graham, A. L. (1994) The inertial lift on a rigid sphere translating in a linear shear flow. *International Journal of Multiphase Flow* **20,** 339–353.

Dandy, D. S. and Dwyer, H. A. (1990) A sphere in a shear flow at finite Reynolds number: effect of shear on particle lift, drag, and heat transfer. *Journal of Fluid Mechanics* **216,** 381–410.

Dennis, S. C. R. and Walker, J. D. A. (1971) Calculation of the steady flow past a sphere at low and moderate Reynolds numbers. *Journal of Fluid Mechanics* **48,** 771–789.

Feuillebois, F. (1980) Certains problèmes d'écoulements mixtes fluides–particules solides. Thèse de l'Université Pierre et Marie Curie, Paris VI, France.

McLaughlin, J. B. (1991) Inertial migration of a small sphere in linear shear flows. *Journal of Fluid Mechanics* **224,** 261–274.

Mei, R. (1992) An approximate expression for the shear lift force on a spherical particle at finite Reynolds number. *International Journal of Multiphase Flow* **18,** 145–147.

Morsi, S. A. and Alexander, A. J. (1972) An investigation of particle trajectories in two-phase flow systems. *Journal of Fluid Mechanics* **55,** 193–208.

Oesterle, B. and Bui Dinh, T. (1998) Experiments on the lift of a spinning sphere in a range of intermediate Reynolds numbers. *Experiments* in *Fluids*, in press.

Patankar, S. V. (1980) *Numerical Heat Transfer and Fluid Flow*, 1st edn, pp. 79–111. Hemisphere, New York.

Payard, M. and Coutanceau, M. (1974) Sur l'étude expérimentale de la naissance et de l'évolution du tourbillon attaché à l'arrière d'une sphère qui se déplace, à vitesse uniforme, dans un fluide visqueux. *C.R. Academie des Sciences, Paris B* **278,** 369–372.

Rubinow, S. I. and Keller, J. B. (1961) The transverse force on a spinning sphere moving in a viscous fluid. *Journal of Fluid Mechanics* **11,** 447–459.

Saffman, P. G. (1965) The lift on a small sphere in a slow shear flow. *Journal of Fluid Mechanics* **22,** 385–400.

Saffman, P. G. (1968) Corrigendum. *Journal of Fluid Mechanics* **31,** 624.

Takagi, H. (1974) On the slow motion of a sphere in a viscous fluid. *Journal of the Physics Society of Japan* **37,** 505–510.

Taneda, S. (1956) *Studies on Wake Vortices (III)*. Experimental investigation of the wake behind a sphere at low Reynolds numbers. Reports of Research Institute for Applied Mechanics, Kyushu University, IV, pp. 99–105.

van Doormaal, J. P. and Raithby, G. D. (1985) An evaluation of the segregated approach for predicting incompressible fluid flows. *ASME Heat Transfer Conference*, Denver, Paper 85-HT-9.

Yamamoto, F., Koukawa, M., Monya, H., Teranishi, A. and Miyamoto, H. (1993) An experimental study of simulation of pneumatic conveying (lift and drag applied to a sphere in high-Reynolds-number linear shear flow). *International Journal of the Japanese Society of Mechanical Engineers, Series B* **36,** 294–295.